The Astrophysical Journal Letters, 826:L17 (5pp), 2016 August 1 doi:10.3847/2041-8205/826/2/L17

THE FIRST SPECTRUM OF THE COLDEST BROWN DWARF

Andrew J. Skemer[1], Caroline V. Morley[1], Katelyn N. Allers[2], Thomas R. Geballe[3], Mark S. Marley[4], Jonathan J. Fortney[1], Jacqueline K. Faherty[5,6,8], Gordon L. Bjoraker[7], and Roxana Lupu[4]
[1] University of California, Santa Cruz, Santa Cruz, 1156 High Street, Santa Cruz, CA 95064, USA
[2] Bucknell University, 701 Moore Avenue, Lewisburg, PA 17837, USA
[3] Gemini Observatory, 670 North A'ohoku Place, Hilo, HI 96720, USA
[4] NASA Ames Research Center, Moffett Field, CA 94035, USA
[5] Carnegie Institute for Science, Department of Terrestrial Magnetism, 5241 Broad Branch Road, NW, Washington, DC 20015, USA
[6] American Museum of Natural History, Central Park West & 79th Street, New York, NY 10024, USA
[7] NASA Goddard Space Flight Center, 8800 Greenbelt Road, Greenbelt, MD 20771, USA
Received 2016 May 14; revised 2016 June 14; accepted 2016 June 23; published 2016 July 25

ABSTRACT

The recently discovered brown dwarf *WISE* 0855 presents the first opportunity to directly study an object outside the solar system that is nearly as cold as our own gas giant planets. However, the traditional methodology for characterizing brown dwarfs—near-infrared spectroscopy—is not currently feasible, as *WISE* 0855 is too cold and faint. To characterize this frozen extrasolar world we obtained a 4.5–5.2 μm spectrum, the same bandpass long used to study Jupiter's deep thermal emission. Our spectrum reveals the presence of atmospheric water vapor and clouds, with an absorption profile that is strikingly similar to Jupiter's. The spectrum quality is high enough to allow for the investigation of dynamical and chemical processes that have long been studied in Jupiter's atmosphere, but now on an extrasolar world.

Key words: brown dwarfs

1. INTRODUCTION

The coldest characterizable exoplanets are still much hotter than the gas giant planets in our solar system (Kuzuhara et al. 2013; Macintosh et al. 2015). However, with the recent discovery of a ~250 K brown dwarf, WISE J085510.83071442.5 (hereafter *WISE* 0855), we now have our first opportunity to directly study an object whose physical characteristics are similar to Jupiter (Luhman 2014). *WISE* 0855 is the nearest known planetary mass object, and the coldest known compact object outside of our solar system (Luhman 2014). Its extremely low temperature makes it the first object after Earth, Mars, Jupiter, and Saturn that is likely to host water clouds in its visible atmosphere (Marley et al. 1999; Sudarsky et al. 2000; Faherty et al. 2014).

A handful of photometric detections and non-detections confirm that W0855 is cold, but they only allow us to speculate on its atmospheric composition (Beamín et al. 2014; Faherty et al. 2014; Kopytova et al. 2014; Wright et al. 2014). *WISE* 0855 is too faint to characterize with conventional spectroscopy in the optical or near-infrared (<2.5 μm). Like Jupiter, a minimum in CH_4 and H_2 gas opacity allows thermal emission from the deep atmosphere to escape through a 5 μm atmospheric window (Low & Davidson 1969; Bjoraker et al. 1986a, 1986b). Spectroscopy at these wavelengths is challenging but not impossible. While there are currently no space-based facilities capable of 5 μm spectroscopy, ground-based telescopes can observe through the Earth's 4.5–5.2 μm atmospheric window, although sensitivity is limited by the brightness of the Earth's sky. With careful calibration, we were able to obtain a spectrum of *WISE* 0855, an object that is five times fainter than the faintest object previously detected with ground-based 5 μm spectroscopy (Geballe et al. 2009; Wright et al. 2014).

[8] Hubble Fellow.

2. OBSERVATIONS

We observed *WISE* 0855 with the Gemini-North telescope and the Gemini Near Infrared Spectrograph (GNIRS; Elias et al. 2006). Gemini-North is located near the summit of Mauna Kea, a cold location that also provides some of the driest conditions of any astronomical site in the world. Because of those attributes, as well as the telescope's low emissivity, the infrared background incident on Gemini's instruments is the lowest of any 8–10 m class telescope. Additionally, Gemini-North is operated in queue-mode, allowing us to observe *WISE* 0855 over many nights in clear, dry and calm conditions. In total, we observed *WISE* 0855 for 14.4 hr over 13 nights. We calibrated the transmission of the Earth's atmosphere by observing standard stars before and after every observation of *WISE* 0855.

GNIRS was configured with its long-wavelength camera, 31.7 line mm^{-1} grating and 0.″675 slit, which provides a single order spectrum covering the M-band (4.5–5.2 μm) at a spectral resolution of $R \sim 800$. Although GNIRS is typically used with its fastest readout mode for broad M-band spectroscopy, we found that there was still appreciable read-noise at some wavelengths, and decided to operate in its second fastest mode, which uses 16 digital averages and has an overhead of 0.6 s per frame. In order to keep our observations of *WISE* 0855 efficient, we integrated for 2.5 s, which is enough to saturate the brightest *M*-band skylines. These wavelengths were then masked in our later analysis.

Observing conditions in the Gemini queue were limited to photometric conditions, <0.″8 seeing at the *V*-band, <3 mm precipitable water vapor, and <1.5 airmass. Telluric calibrators (HIP 39898 and HIP 49900) were obtained at similar airmasses before and after each observation, with a maximum separation of 2 hr.

Because *WISE* 0855 is essentially invisible in the near-infrared (Beamín et al. 2014; Faherty et al. 2014; Kopytova et al. 2014), acquisitions were done using a blind offset from a

Table 1
Observations

Date	*WISE* 0855 Airmass	IQ	WV	Telluric	Telluric Airmass
2015 Dec 01	1.29	20%	50%	HIP 39898	1.35
2015 Dec 01	1.16	20%	50%	HIP 49900	1.22
2015 Dec 01	1.14	20%	50%	HIP 49900	1.13
2015 Dec 03	1.26	20%	50%	HIP 39898	1.31
2015 Dec 03	1.15	20%	50%	HIP 49900	1.20
2015 Dec 05	1.13	20%	20%	HIP 39898	1.17
2015 Dec 05	1.15	20%	20%	HIP 49900	1.12
2015 Dec 06	1.18	70%	20%	HIP 39898	1.22
2015 Dec 06	1.13	70%	20%	HIP 49900	1.14
2015 Dec 07	1.13	20%	20%	HIP 39898	1.17
2015 Dec 14	1.32	70%	20%	HIP 39898	1.39
2015 Dec 14	1.17	70%	20%	HIP 49900	1.24
2015 Dec 29	1.14	70%	20%	HIP 39898	1.19
2015 Dec 29	1.13	70%	20%	HIP 49900	1.13
2015 Dec 30	1.14	70%	20%	HIP 39898	1.19
2015 Dec 30	1.13	70%	20%	HIP 49900	1.13
2015 Dec 30	1.28	70%	20%	HIP 49900	1.13
2015 Dec 31	1.23	70%	20%	HIP 39898	1.30
2016 Jan 01	1.29	20%	20%	HIP 39898	1.38
2016 Jan 02	1.25	70%	20%	HIP 39898	1.29
2016 Jan 03	1.29	70%	20%	HIP 39898	1.33
2016 Jan 03	1.19	70%	20%	HIP 49900	1.32
2016 Jan 05	1.26	70%	20%	HIP 39898	1.34
2016 Jan 05	1.15	70%	20%	HIP 49900	1.20

Note. IQ and WV refer to Gemini's image quality and precipitable water vapor observational constraint boundaries (https://www.gemini.edu/node/10781).

nearby star (08 55 07.73–07 14 28.0, J2000.0) with a recent astrometric calibration (Faherty et al. 2014). The position of *WISE* 0855 was calculated by propagating its proper motion and parallax (Luhman & Esplin 2014). Gemini's offset pointing is accurate to ∼0.″2, and our position estimate for *WISE* 0855 is accurate to ∼0.″1. Thus, it is possible that *WISE* 0855 was slightly misaligned with the slit. However, we chose an oversized slit (0.″675) to mitigate the effects of a slight misalignment. To enable subtraction of the thermal background, we took observations in an ABBA pattern, nodding 6″ along the slit. A data set of *WISE* 0855 consists of 9 ABBA sequences for a total of 36 images and 36 minutes of integration time. In total, we obtained 24 of these data sets for a combined integration time of 14.4 hr. A summary of the dates, conditions, and telluric calibrators for our observations is listed in Table 1.

3. REDUCTIONS

We reduced the data using a modified version of the REDSPEC package[9] to spatially and spectrally rectify each exposure with the dispersion direction as "rows" and the spatial direction as "columns."

For each data set, we first create a nonlinearity flag image by marking pixels with values greater than 10,000 counts per coadd. We then median-scale the images and create nod-subtracted A–B pairs.

Observations of the telluric standards are used to create the spatial and spectral maps, which are then used to rectify the *WISE* 0855 data. The spatial rectification process uses a subtracted A–B pair of telluric star exposures, fits Gaussians to find the center of each star as a function of wavelength, and then fits a second order polynomial to define a trace. These traces are then used to remap each exposure so that the dispersion direction lies along detector rows. To wavelength calibrate and spectrally rectify our exposures, we use sky emission lines in our telluric standard spectra. We determined the wavelengths of 11 skylines by smoothing a model of the sky background for Mauna Kea[10] to match the $R \sim 800$ resolution of our GNIRS spectra. We use a second order polynomial to fit a dispersion solution to each spectral trace, which is then used to remap each exposure so that each column corresponds to a single wavelength. The residuals for our dispersion fits are <2 pixels, or 0.0013 μm.

For each rectified A–B pair image, we remove residual skylines from each column by subtracting that column's median value. We combine the rectified, background-subtracted A–B pairs with a 3-σ clipped mean at each pixel. The uncertainty of each pixel in the stacked image is the standard deviation of the mean.

To extract the spectrum, we create a wavelength-collapsed spatial cut by taking the median of each row in the stacked A–B image, and boxcar-smoothing the profile by 5 pixels (0.″25). We identify the location of the A and B spectra by fitting two Gaussians to the spatial cut. We then extract each spectrum using an aperture radius of $\sim 1.6\sigma$ (where σ is the width of the Gaussian fit to the spatial cut), and subtract any residual sky background by fitting a line to the background regions. If a pixel that was flagged as nonlinear falls in the aperture, the spectrum at that wavelength is also flagged. For each data set, our reduction results in an A and a B spectrum. We extract the spectra of our telluric standard stars using a similar process.

We divide each extracted spectrum of *WISE* 0855 by the spectrum of an adjacent telluric standard, and multiply by an appropriate blackbody. When using the calibrator HIP 39898, there is an additional step to remove its Pfund β emission by fitting and subtracting a Gaussian. In most cases, the airmass of our *WISE* 0855 observation matched the airmass of the telluric observation to within 0.1. In total, we have 48 telluric calibrated spectra of *WISE* 0855, which we combine using a robust weighted mean (Cushing et al. 2004).

We binned the data in 20 pixel increments for presentation in this paper (spectral resolution of ∼300 per point, or ∼150 for Nyquist sampling). Within each bin, we calculated the weighted average and weighted error, which has the effect of suppressing wavelengths with large telluric emission (and low transmission) features. Our calibrated spectrum of *WISE* 0855 is presented in Figure 1. For subsequent spectrum plots in this paper, identical weights are applied to comparison spectra, and are used to calculate each bin's effective wavelength.

In addition to making the spectrum intelligible, binning the data smooths wavelength mismatch errors between *WISE* 0855 and the telluric calibrators, which would result from *WISE* 0855 being slightly misaligned in the oversized slit. To confirm that the wavelength mismatch errors did not affect our final spectrum, we re-reduced the data assuming a 0.″2 slit misalignment for *WISE* 0855 and found negligible differences.

The overall quality of our data reduction process and telluric correction is validated by dividing the spectra of our pre- and post-observation telluric calibrators, averaged over the 13

[9] http://www2.keck.hawaii.edu/inst/nirspec/redspec

[10] http://www.gemini.edu/sciops/telescopes-and-sites/ observing-condition-constraints/ir-background-spectra

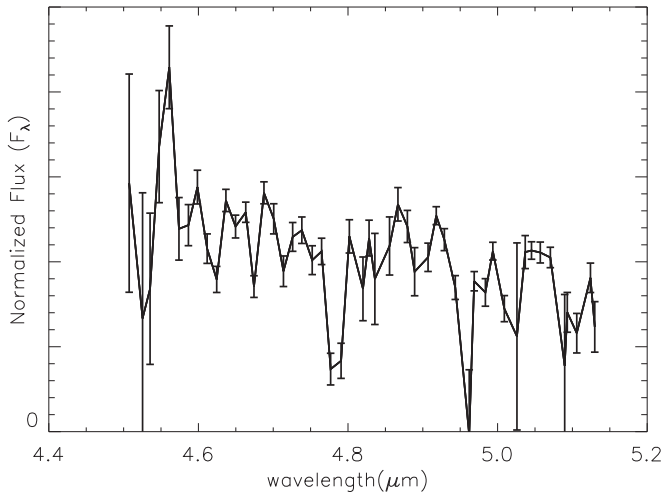

Figure 1. Gemini/GNIRS spectrum of *WISE* 0855 showing numerous absorption features. The spectrum is normalized due to the flux calibration uncertainty associated with blind-offset slit misalignment.

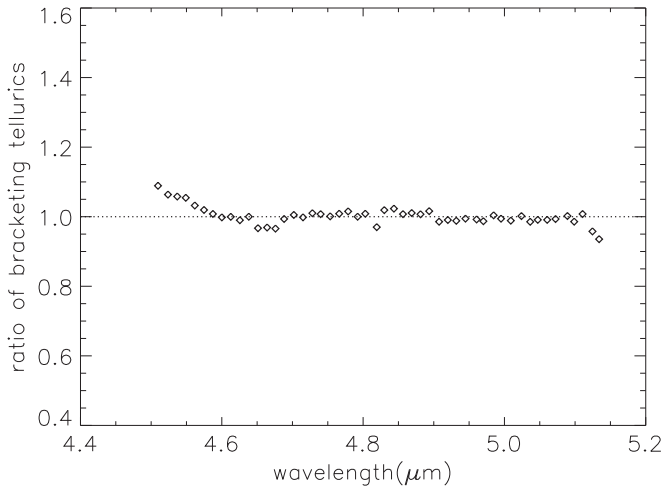

Figure 2. Ratio of the telluric standard spectra observed before and after *WISE* 0855. From 4.6 to 5.1 μm the spectrum is flat with a standard deviation of 2.5%, implying that the errors in the telluric correction are negligible compared to the photon-noise-dominated errors in our *WISE* 0855 spectrum. From 4.5 to 4.6 and 5.1–5.15 μm, the telluric calibration is slightly worse, but still smaller than the reported errors in the *WISE* 0855 spectrum. The data in this figure are binned with the same weighted average as the *WISE* 0855 spectra, and have been normalized to 1.

nights of observations. Figure 2 shows that the ratio of the telluric standards is flat to within 2.5% from 4.6 to 5.1 μm, with slightly larger errors from 4.5–4.6 to 5.1–5.15 μm. In all cases, the telluric mismatch is negligible compared to the background photon noise seen in our spectrum.

4. DESCRIPTION OF ATMOSPHERE MODELS

We interpret the observed spectrum of *WISE* 0855 using custom atmospheric models. All of our models have an effective temperature of 250 K, which is well-constrained from *WISE* 0855s measured luminosity and a radius estimate that is relatively insensitive to unknown parameters, such as *WISE* 0855s age (Luhman 2014).

We calculate cloud-free 1D pressure–temperature profiles assuming both chemical and radiative-convective equilibrium. The thermal radiative transfer is determined using the "source

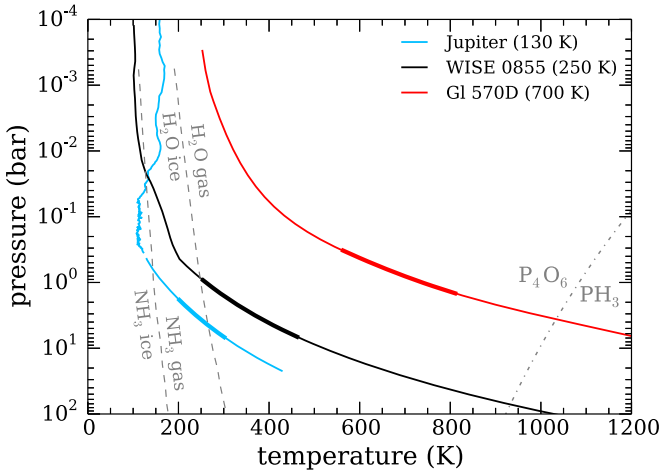

Figure 3. Temperature–pressure profiles of Jupiter (Seiff et al. 1998), *WISE* 0855, and what was previously the coldest extrasolar object with a 5 μm spectrum, Gl 570D (Sorahana & Yamamura 2012). The approximate locations of each object's 5 μm photosphere are denoted with thicker lines (for Jupiter, the photosphere is as seen through cloud-free hot-spots). Two dashed lines show the boundaries where H_2O gas and NH_3 gas begin to condense into clouds composed of H_2O ice and NH_3 ice. A dot–dashed line divides the regions where phosphorous is primarily in P_4O_6 vs. PH_3 under equilibrium chemistry assumptions. *WISE* 0855 and Jupiter have relatively similar temperature–pressure profiles, with photospheres that are in the vicinity of the condensation points for NH_3 and H_2O.

function technique" presented in Toon et al. (1989). The gas opacity is calculated using correlated-k coefficients; our opacity database is described extensively in Freedman et al. (2008) and Freedman et al. (2014). The atmosphere models are more extensively described in McKay et al. (1989), Marley et al. (1996), Marley et al. (1999), Marley et al. (2002), Fortney et al. (2008), and Saumon & Marley (2008).

Exoplanets and brown dwarfs that are cooler than ~350 K are expected to form water ice clouds in their upper atmospheres, which are optically thick enough to alter the emergent spectrum (Marley et al. 1999; Sudarsky et al. 2000; Burrows et al. 2003; Morley et al. 2014). We find that partly cloudy models (Morley et al. 2014) are indistinguishable from cloud-free models after normalizing and binning over the wavelength range of our *WISE* 0855 spectrum. Radiative-convective equilibrium models with full water cloud coverage do not converge well between $T_{\rm eff} \sim$ 200 and 450 K (Morley et al. 2014).

For this reason, we use a simplified approach to consider the effect of clouds at different layers, following studies of Jupiter's mid-infrared spectral features (Bjoraker et al. 2015). We calculate the pressure–temperature profile of a cloud-free atmosphere in radiative-convective equilibrium. We then use that profile and calculate the thermal emission using an adapted version of `DISORT` (Morley et al. 2015) including a gray, fully absorbing cloud with optical depth $\tau = 1$. We vary the cloud-top pressure of this gray cloud to best match the observed spectrum of *WISE* 0855.

We also use the `DISORT` radiative transfer scheme to model the effect of non-equilibrium abundances of trace gases such as PH_3 and CH_3D. We first calculate a cloud-free profile in chemical equilibrium, and then calculate spectra in which we change the abundance of each gas separately, changing the mixing ratio of that gas to be uniform at that value throughout the atmosphere.

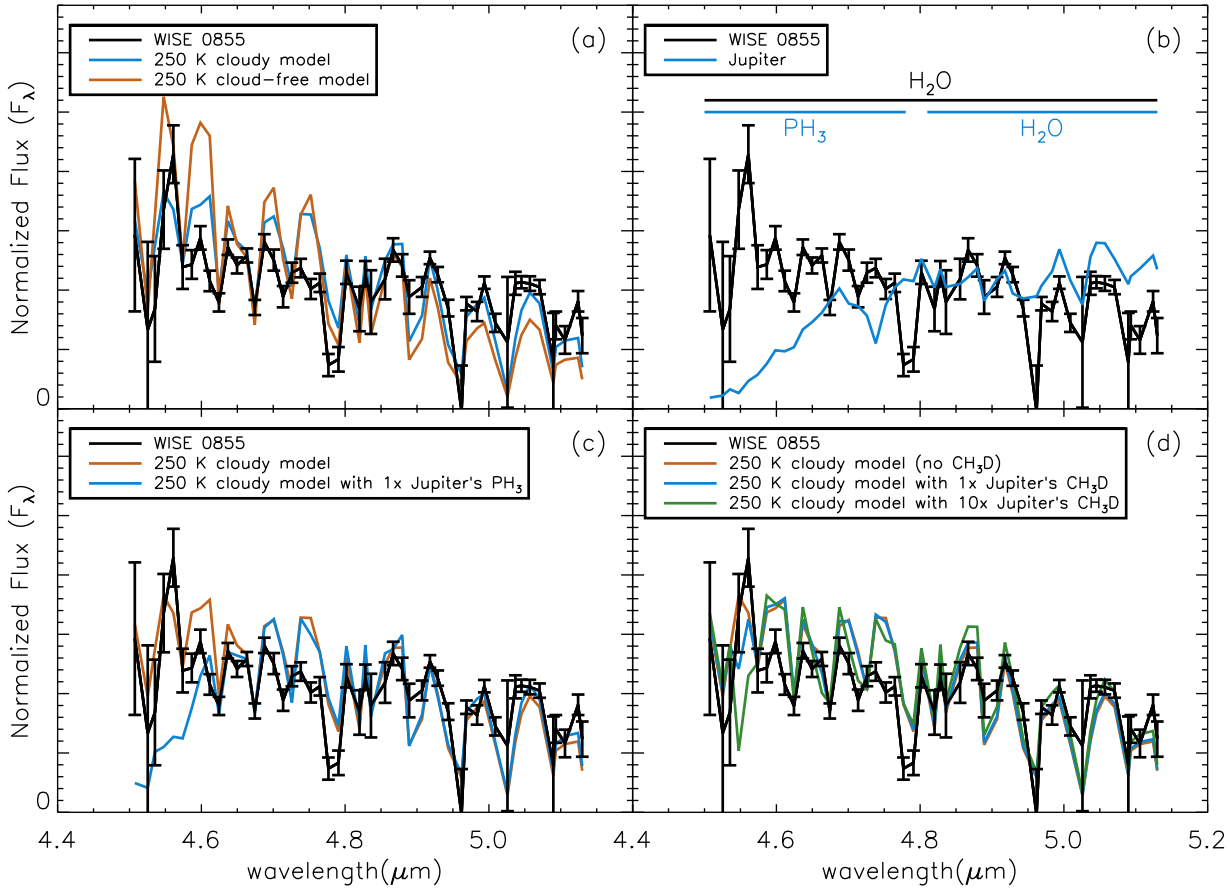

Figure 4. (a) Gemini/GNIRS spectrum of *WISE* 0855 compared to 250 K cloudy and cloud-free brown dwarf models. The locations of the absorption features match well between the data and models, and are all consistent with water vapor. The shapes of the absorption features are affected by clouds (likely H_2O), which mute the spectrum, providing a better fit between the model and the data than the cloud-free case. The remaining discrepancies between the cloudy model and the data are likely due, in part, to additional complexities (such as three-dimensional structures) of the clouds. (b) Gemini/GNIRS spectrum of *WISE* 0855 compared to a full-disk spectrum of Jupiter from the *Infrared Space Observatory* (*ISO*; Encrenaz et al. 1996), binned to *WISE* 0855's resolution. The spectra show striking similarities from 4.8 to 5.2 μm, as both objects are dominated by H_2O (there is a slope offset because Jupiter is colder than *WISE* 0855, and a notable discrepancy at 4.96 μm). From 4.5 to 4.8 μm, Jupiter's spectrum is dominated by PH_3, which has been used to infer turbulent diffusion of hot material from deep in Jupiter's atmosphere (Prinn & Lewis 1975; Kunde et al. 1982; Visscher et al. 2006). The *WISE* 0855 spectrum does not show a similar PH_3 feature. (c) Gemini/GNIRS spectrum of *WISE* 0855 compared to models with equilibrium chemistry PH_3, and enhanced PH_3 to match the abundance measured in Jupiter. The *WISE* 0855 spectrum is strongly inconsistent with the enhanced PH_3 model, suggesting that *WISE* 0855 does not have the same turbulent mixing seen on Jupiter. (d) Gemini/GNIRS spectrum of *WISE* 0855 compared to models that vary CH_3D abundance. The *WISE* 0855 spectrum has the raw sensitivity to measure CH_3D at 4.55 μm, but the imperfect match between the rest of the spectrum and our current model would hamper an analysis.

Our model temperature–pressure profile for *WISE* 0855 and the next coldest brown dwarf with a 5 μm spectrum (Gl 570D; 700 K Sorahana & Yamamura 2012) are shown in Figure 3, along with a measured profile for Jupiter (Seiff et al. 1998) extrapolated along an adiabat to lower depths. Jupiter and *WISE* 0855 have relatively similar temperature–pressure profiles, thus their photospheres should display similar features. Both photospheres are near the condensation temperatures for H_2O and NH_3 clouds. Under equilibrium chemistry assumptions, neither photosphere should have detectable amounts of PH_3.

5. DISCUSSION

5.1. Composition and Clouds

Our equilibrium chemistry models from Section 4 predict that for a 250 K object, all of the major absorption features from 4.5 to 5.2 μm are the result of water vapor. Figure 4(a) shows cloudy and cloud-free models compared to the *WISE* 0855 spectrum. The wavelengths of the model features match the wavelengths of the spectrum features, which suggests that our *WISE* 0855 spectrum is dominated by water vapor.

The cloudy model is a better fit to the depths of *WISE* 0855's absorption features, as well as its overall slope. While our model does not specify a particular cloud composition, *WISE* 0855 is at a temperature where the clouds are likely to be composed of water or water ice (Burrows et al. 2003; Morley et al. 2012). The cloudy model's fit to *WISE* 0855 is imperfect, which suggests that there is additional complexity that is beyond the scope of our current models. For example, the particular vertical and horizontal structure of the clouds is likely to impact *WISE* 0855s appearance.

5.2. Comparison with Jupiter

We compare our spectrum of *WISE* 0855 to a full-disk spectrum of Jupiter in Figure 4(b). From 4.8 to 5.2 μm, *WISE* 0855 and Jupiter are strikingly similar, as Jupiter's atmosphere is also dominated by H_2O absorption at these wavelengths (Kunde et al. 1982). From 4.5 to 4.8 μm, Jupiter's

spectrum is dominated by PH_3 (phosphine) absorption (Kunde et al. 1982). If Jupiter were in chemical equilibrium, phosphorous would exist in the form of P_4O_6 in its photosphere and PH_3 in its hotter interior (Prinn & Lewis 1975; Visscher et al. 2006). The existence of PH_3 in Jupiter's spectrum is evidence that Jupiter's atmosphere turbulently mixes gases from its hot interior into its cooler photosphere on a faster timescale than the $PH_3 \rightarrow P_4O_6$ reaction sequence can reach equilibrium (Prinn & Lewis 1975; Visscher et al. 2006).

5.3. PH_3 Chemistry and Mixing

WISE 0855s spectrum does not show the strong PH_3 absorption seen in Jupiter's spectrum. In Figure 4(c), we show our equilibrium chemistry model for *WISE* 0855, along with a model that has PH_3 enhanced to the abundance measured in Jupiter (Lodders 2010). If *WISE* 0855 had Jupiter's abundance of PH_3, it would easily be visible in our spectrum. The fact that *WISE* 0855 has less PH_3 than Jupiter most likely implies that *WISE* 0855 has less turbulent mixing than Jupiter, although atmospheric metallicity and gravity may also play a role.

5.4. Deuterium

Figure 4(d) shows a comparison of *WISE* 0855 with models that vary CH_3D (deuterated methane). Deuterium is expected to be quickly depleted by fusion in objects more massive than $\sim$13 M_{jup}, a boundary commonly used to separate planets from brown dwarfs (Burrows et al. 1997; Spiegel et al. 2011). Thus, CH_3D measurements can be used to glean information about the masses of exoplanets and free-floating planets/brown dwarfs. In our solar system, deuterium becomes chemically concentrated in certain environments, and has been used to study the formation of the giant planets, and the delivery of water to Earth (Owen et al. 1986; Altwegg et al. 2015). In multi-planet extrasolar systems, CH_3D measurements could similarly be used to study the composition of the planets' nascent materials.

Our spectrum has the sensitivity to distinguish between models with Jupiter's approximately primordial deuterium abundance (Owen et al. 1986; Lodders 2010), and models with no deuterium. However, the CH_3D absorption feature is blended with water absorption features, which need to be better understood before we can really measure CH_3D.

6. FUTURE PROSPECTS

To understand the nature of clouds and vertical mixing in cold gas giants, we need 5 μm spectra of objects across a continuum of temperatures. After Jupiter (130 K) and *WISE* 0855 (250 K), the next coldest object with a 5 μm spectrum is Gl 570D (700 K) (Sorahana & Yamamura 2012). In the near term, ground-based telescopes have the sensitivity to obtain spectra of a handful of objects in this temperature range. Future facilities, like the *James Webb Space Telescope*, will have the sensitivity to characterize cold gas giants with higher precision, and at wavelengths not possible from Earth (Morley et al. 2014). The next generation of ground-based telescopes (Extremely Large Telescopes) will have the angular resolution and sensitivity to study systems with multiple exoplanets that look like *WISE* 0855. With spectrographs operating in the 5 μm atmospheric window (Skemer et al. 2015), it will be possible to compare large samples of exoplanets at wavelengths that have revealed much of what we know about gas giants in our own solar system.

This work is based on observations obtained at the Gemini Observatory, which is operated by the Association of Universities for Research in Astronomy, Inc., under a cooperative agreement with the NSF on behalf of the Gemini partnership: the National Science Foundation (United States), the National Research Council (Canada), CONICYT (Chile), Ministerio de Ciencia, Tecnología e Innovación Productiva (Argentina), and Ministério da Ciência, Tecnologia e Inovação (Brazil). The authors thank Mike Cushing and Pat Irwin for supplying compiled spectroscopy of Jupiter, Satoko Sorahana for supplying AKARI spectroscopy of T dwarfs, Michelle Edwards for advice about Gemini scheduling, and the anonymous referee for a helpful report.

REFERENCES

Altwegg, K., Balsiger, H., Bar-Nun, A., et al. 2015, Sci, 347, 1261952
Beamín, J. C., Ivanov, V. D., Bayo, A., et al. 2014, A&A, 570, L8
Bjoraker, G. L., Larson, H. P., & Kunde, V. G. 1986a, ApJ, 311, 1058
Bjoraker, G. L., Larson, H. P., & Kunde, V. G. 1986b, Icar, 66, 579
Bjoraker, G. L., Wong, M. H., de Pater, I., & Ádámkovics, M. 2015, ApJ, 810, 122
Burrows, A., Marley, M., Hubbard, W. B., et al. 1997, ApJ, 491, 856
Burrows, A., Sudarsky, D., & Lunine, J. I. 2003, ApJ, 596, 587
Cushing, M. C., Vacca, W. D., & Rayner, J. T. 2004, PASP, 116, 362
Elias, J. H., Joyce, R. R., Liang, M., et al. 2006, Proc. SPIE, 6269, 62694C
Encrenaz, T., de Graauw, T., Schaeidt, S., et al. 1996, A&A, 315, L397
Faherty, J. K., Tinney, C. G., Skemer, A., & Monson, A. J. 2014, ApJL, 793, L16
Fortney, J. J., Lodders, K., Marley, M. S., & Freedman, R. S. 2008, ApJ, 678, 1419
Freedman, R. S., Lustig-Yaeger, J., Fortney, J. J., et al. 2014, ApJS, 214, 25
Freedman, R. S., Marley, M. S., & Lodders, K. 2008, ApJS, 174, 504
Geballe, T. R., Saumon, D., Golimowski, D. A., et al. 2009, ApJ, 695, 844
Kopytova, T. G., Crossfield, I. J. M., Deacon, N. R., et al. 2014, ApJ, 797, 3
Kunde, V., Hanel, R., Maguire, W., et al. 1982, ApJ, 263, 443
Kuzuhara, M., Tamura, M., Kudo, T., et al. 2013, ApJ, 774, 11
Lodders, K. 2010, Geochemical News, 142, https://www.geochemsoc.org/publications/geochemicalnews/gn142jan10/atmosphericchemistryoftheg/
Low, F. J., & Davidson, A. W. 1969, BAAS, 1, 200
Luhman, K. L. 2014, ApJL, 786, L18
Luhman, K. L., & Esplin, T. L. 2014, ApJ, 796, 6
Macintosh, B., Graham, J. R., Barman, T., et al. 2015, Sci, 350, 64
Marley, M. S., Gelino, C., Stephens, D., Lunine, J. I., & Freedman, R. 1999, ApJ, 513, 879
Marley, M. S., Saumon, D., Guillot, T., et al. 1996, Sci, 272, 1919
Marley, M. S., Seager, S., Saumon, D., et al. 2002, ApJ, 568, 335
McKay, C. P., Pollack, J. B., & Courtin, R. 1989, Icar, 80, 23
Morley, C. V., Fortney, J. J., Marley, M. S., et al. 2012, ApJ, 756, 172
Morley, C. V., Fortney, J. J., Marley, M. S., et al. 2015, ApJ, 815, 110
Morley, C. V., Marley, M. S., Fortney, J. J., et al. 2014, ApJ, 787, 78
Owen, T., Lutz, B. L., & de Bergh, C. 1986, Natur, 320, 244
Prinn, R. G., & Lewis, J. S. 1975, Sci, 190, 274
Saumon, D., & Marley, M. S. 2008, ApJ, 689, 1327
Seiff, A., Kirk, D. B., Knight, T. C. D., et al. 1998, JGR, 103, 22857
Skemer, A. J., Hinz, P., Montoya, M., et al. 2015, Proc. SPIE, 9605, 96051D
Sorahana, S., & Yamamura, I. 2012, ApJ, 760, 151
Spiegel, D. S., Burrows, A., & Milsom, J. A. 2011, ApJ, 727, 57
Sudarsky, D., Burrows, A., & Pinto, P. 2000, ApJ, 538, 885
Toon, O. B., McKay, C. P., Ackerman, T. P., & Santhanam, K. 1989, JGR, 94, 16287
Visscher, C., Lodders, K., & Fegley, B., Jr. 2006, ApJ, 648, 1181
Wright, E. L., Mainzer, A., Kirkpatrick, J. D., et al. 2014, AJ, 148, 82